Metalurgi (2022) 1: 7 - 14

METALURGI
Majalah Ilmu dan Teknologi
p-ISSN 0126-3188 | e-ISSN 2443-3926
ejurnalmaterialmetalurgi.lipi.go.id

DYNAMIC PLASTIC DEFORMATION INDUCED BY REPETITIVE HAMMERING ON CR-MN AUSTENITIC STAINLESS STEEL

Syahwira Taqwa Triadi[a], Cherly Selindiana[a], Hermawan Judawisastra[b,*], Aditianto Ramelan[b]

[a] Material Science and Engineering Program Study
[b] Material Science and Engineering Research Group
Faculty of Mechanical and Aerospace Engineering, Bandung Institute of Technology
Jl. Ganesha 10 Bandung, Indonesia 40132
*E-mail: Hermawan.Judawisastra@material.itb.ac.id

Received : 22-12-2021, Revised : 15-04-2022, Accepted : 23-06-2022

Abstract

Austenitic stainless steels have advantages, such as high ductility and good corrosion resistance. The cold working process can increase the hardness and strength of the material. However, because a metastable austenite phase occurs in that material, there is a phase change of γ austenite to α'-martensite and ε-martensite, which will reduce the ductility and its corrosion resistance. The strengthening process with DPD (dynamic plastic deformation) can prevent the formation of martensitic phases through repeated impact at high strain rates. This study analyzed microstructures and hardness evaluation on Cr-Mn austenitic stainless steel due to dynamic plastic deformation through the repetitive hammering method. Repetitive hammering with a strain rate of 6,2 s^{-1} on Cr-Mn austenitic stainless steels was carried out on five specimens with variations in the impact of 50, 100, 150, 250, and 350 times with impact energy of 486 J/cm^2; 2.207 J/cm^2; 2.569 J/cm^2; 6.070 J/cm^2; and 11.330 J/cm^2 respectively. Microstructure, hardness, and XRD (x-ray diffraction) analyses were carried out on Cr-Mn austenitic stainless steels before and after repetitive hammering. Metallography was carried out to observe the microstructure using an optical microscope. The hardness was tested through the Rockwell A hardness test. XRD examination was used to identify the phases formed and indications of nano-twins. The repetitive hammering process up to 350 times has succeeded in increasing hardness from 53.5 HRA to 71.6 HRA. Plastic deformation introduced by repetitive hammering produced slip bands, cross bands, wavy bands, and an indication of nano-twins formation and increased hardness.

Keywords: *DPD (dynamic plastic deformation), repetitive hammering, nano-twins, Cr-Mn austenitic stainless steel, SFE (stacking fault energy)*

1. INTRODUCTION

Austenitic stainless steel is widely used due to its good corrosion resistance, formability, and weldability. However, austenitic stainless steel relatively has low mechanical properties compared to other types of steel (around 100-400 MPa) due to its FCC (face center cubic) structure [1]–[4]. To enhance its mechanical properties, cold working is commonly used on austenitic stainless steel to create high strength martensite phase. However, martensite formation on the austenitic stainless steel could reduce its corrosion resistance [5]-[6].

In the previous study carried out on the 316L austenitic stainless steel [7], a high strain rate is needed to prevent the formation of the martensite phase and maintain austenitic stainless steel with high ductility and good corrosion resistance [7]-[8]. With a high strain rate, the phenomenon is mechanical twinning with the formation of nano-twin grains in austenitic stainless steels [7], [9]. The volume fraction of the nano-twin is about 8% in austenitic stainless steels, increasing the yield strength of the material by more than 25% [11]. One method for forming nano-twin is dynamic plastic deformation (DPD) [7], [11]-[14].

The formation of the nano-twin will be influenced by the material's SFE (stacking fault energy) value. The mechanical twinning phenomenon will be activated if the stacking

DOI : 10.14203/metalurgi.v37i1.618

Metalurgi is Sinta 2 Journal (https://sinta.ristekbrin.go.id/journals/detail?id=3708) accredited by Ministry of Research & Technology, Republic of Indonesia

fault energy is between 20 to 50 mJ/m^2, below which martensite formation is more accessible [15]. In addition, austenitic stainless steel material has a metastable austenite phase that is easily transformed into martensite when cold working at temperatures farther away from Md_{30} [16]- [17]. Md_{30} is the temperature at which 50% martensite is formed after 30% true strain. Thus, as the temperature gets colder and closer to the Md_{30} temperature, the austenite is more stable and difficult to transform into α'-martensite or ε-martensite in austenitic stainless steels [16].

In this study, dynamic plastic deformation DPD was carried out using low-cost laboratory-made repetitive hammering, which has the working principle of repeatedly dropping the load on the specimen. Then we will study dynamic plastic deformation treatment through the repetitive hammering method on austenitic Cr-Mn stainless steel material with manganese as a substitute of nickel as an austenite former [18]. After the repetitive hammering process, its microstructure and hardness were analyzed to prove the strengthening mechanism of the Cr-Mn austenitic stainless steel through this treatment.

2. MATERIALS AND METHODS

2.1 Materials

Cr-Mn austenitic stainless steel with 10% Mn and 13% Cr was used in this study.

Table 1. Actual chemical composition of Cr-Mn austenitic stainless steel

Elements (wt%)							
C	**Si**	**S**	**P**	**Mn**	**Ni**	**Cr**	**Fe**
0.058	0.36	0.017	0.049	10.468	1.26	13.63	73.22

The specimen's chemical composition was characterized through OES (optical emission spectroscopy), as shown in Table 1.

2.2 Methods

The following equations (1) and (2) are used to calculate the value of SFE (stacking fault energy) [4], [8], [18], and Md_{30} temperature [16]-[17].

$$\text{SFE (mJ/m}^2\text{)} = 2{,}2 + 1{,}9\text{Ni} - 2{,}9\text{Si} + 0{,}77\text{Mo} + 0{,}5\text{Mn} + 40\text{C} - 0{,}016\text{Cr} - 3{,}6\text{N} \quad (1)$$

$$Md_{30}\text{, Angel} = 413 - 462\,(\text{C+N}) - 9.2\text{Si} - 8.1\text{Mn} - 13.7\text{Cr} - 9.5\text{Ni} - 18.5\text{Mo} \quad (2)$$

Solution annealing treatment was conducted to eliminate the deformation process on the as-received specimen at 1050 °C for 2 hours [19]. After solution annealing treatment, dynamic plastic deformation was conducted through the repetitive hammering method. Repetitive hammering with a strain rate of 6.2 s^{-1} on Cr-Mn austenitic stainless steels was carried out on five specimens with variations in the impact of 50, 100, 150, 250, and 350 times using 4.95 kg load mass as shown in the scheme in Fig. 1.

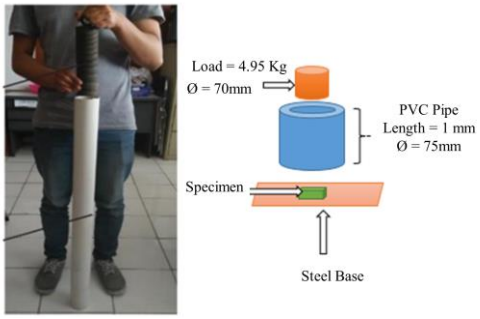

Figure 1. Repetitive hammering process

Hammering energy (E') and true strain (ε_t) on each specimen were calculated through equations (3) and (4). With, n = hammering cycle number, m = load (4.95 kg), g = gravity constant, h = Hammering drop height (1 m), dan s = specimen contact area, t_0= specimen's initial thickness, t_f= specimen's final thickness

$$E' = \frac{n.m.g.h}{s} \quad (3)$$

$$\varepsilon_t = ln\frac{t_0}{t_f} \quad (4)$$

Microstructure observation was conducted through the metallography examination. The specimens were polished and etched with aqua regia etchant to reveal their microstructure. Then, a hardness test was done with Rockwell A hardness test. Lastly, the XRD (x-ray diffraction) examination analyzed the specimen's existing phase.

3. RESULT AND DISCUSSION

The OES (optical emission spectroscopy) characterization results in Table 1, the material used belongs to the low alloy austenitic stainless-steel Cr-Mn. The composition of Ni as a stabilizer of austenite is relatively low, but the function of Ni is replaced by Mn so that the composition is relatively high. Reducing the composition of Ni by 1% must be replaced by adding 2% Mn to achieve austenite stability [20]–[24].

The Md_{30} and SFE (stacking fault energy) values are 99.2 °C and 0.0109 J/cm^2, respectively, indicating the very low possibility of martensite formation at room temperature during deformation [16].

Microplastic deformation marks and twinning were already observed on the as-received microstructure, indicating that the materials were already plastically deformed. Microplastic deformation twinning was successfully reduced with solution annealing treatment due to recrystallization, as shown in Fig. 2.

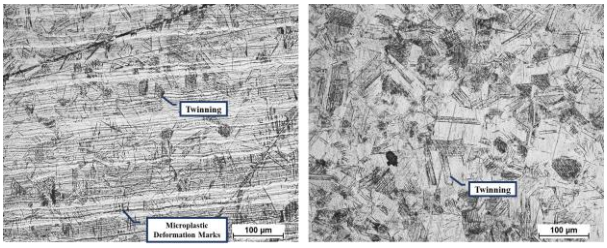

(a) (b)

Figure 2. Microstructure of (a) as received and (b) after solution annealing with aqua regia etchant low alloy austenitic stainless-steel Cr-Mn

Based on energy calculation and dimensional measurement on the austenitic stainless-steel Cr-Mn before and after repetitive hammering, more hammering from 50 to 350 cycles increase the hammering energy, reduce specimen thickness, and increase the true strain, as shown in Table. 2. Hammering energy achieved is much higher than the required (SFE) of materials (0.0109 J/cm^2) calculated using Equation 1.

Table 2. Hammering energy and true strain of low alloy austenitic stainless-steel Cr-Mn after repetitive hammering

Cycle (n)	Hammering Energy (J/cm^2)	Initial thickness (mm)	Final thickness (mm)	True Strain
50	486		9.00	0.03
100	2207		8.67	0.07
150	2569	9.30	8.14	0.13
250	6070		7.74	0.18
350	11330		6.88	0.30

Increased the true strain of materials is the primary indicator of a higher degree of plastic deformation due to higher hammering energy. After repetitive hammering, slip band and cross-band were observed on the microstructure of the 486 J/cm^2 hammering energy or 50 hammering cycle. The density of the slip band was increased along with the greater hammering energy. Furthermore, the wavy band was observed on austenitic stainless steel Cr-Mn microstructure that received higher hammering energy as in 150 Hammering Cycle (2569 J/cm^2 Hammering Energy) and 350 Hammering Cycle (11330 J/cm^2 Hammering Energy), while twinning phenomena were observed on all of austenitic stainless steel Cr-Mn. Slip bands and cross-band were easily formed on the austenitic stainless steel that received repetitive hammering due to its low SFE value; thus, both slip bands and cross-band will be formed on the material that experienced lower hammering energy [25]–[28].

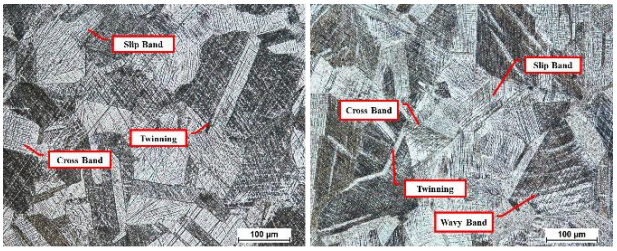

(a) (b)

Figure 3. Microstructure of 50 hammering cycle (486 J/cm^2 hammering energy) and (b) 150 hammering cycle (2569 J/cm^2 hammering energy) with aqua regia etchant

After repetitive hammering, plastic deformation on the specimen was confirmed by a metallography examination that showed a higher degree of slip-band and twinning inside the structure grain on the specimen that received higher hammering energy, as shown in Fig. 3 and Fig. 4.

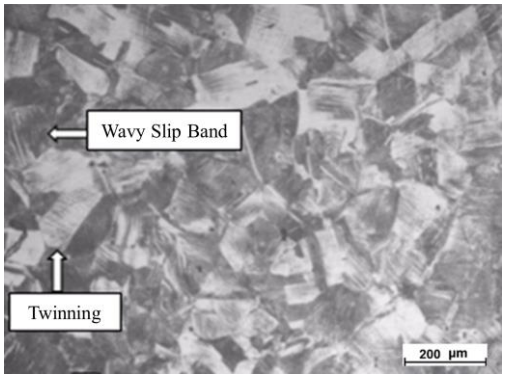

Figure 4. Microstructure of low alloy austenitic stainless-steel Cr-Mn 350 hammering cycle (11330 J/cm^2 hammering energy) with aqua regia etchant

In contrast, a higher SFE is needed to create a wavy band could explain why it is only observed on the higher hammering energy, such as on the 2569 J/cm^2 hammering energy.

The formation of the slip, cross, and wavy bands could obstruct the dislocation movement and cause strain hardening [29]–[31]. This phenomenon was observed in the hardness test result shown in Table 3. The hardness of the stainless steel that was already reduced due to solution annealing treatment from 58 to 53.5 HRA will be increased up to 71.6 HRA after the repetitive hammering process and following the increment of true strain, as shown in Fig. 5.

The XRD analysis in Fig. 6 shows a decreasing austenitic peak (γ-111) intensity from 907 at the as-received to 542 at the material with 350 hammering cycles (11030 J/cm2 hammering energy).

Table 3. Hardness test result of as received, after solution annealing and after repetitive hammering low alloy austenitic stainless-steel Cr-Mn

Specimen / Cycle (n)	Hammering Energy (J/cm^2)	True Strain	Hardness (HRA)
As Received	-	-	58±1.57
After Solution Annealing	-	-	53.5±0.85
50	486	0.03	54.3 ± 0.81
100	2207	0.07	58 ± 1.60
150	2569	0.13	62.2 ± 0.55
250	6070	0.18	67.6 ± 0.38
350	11330	0.30	71.6 ± 0.36

The decreased intensity indicated the formation of the lattice distortion that formed the slip band [11], [29], [32]-[33]. Also, with hammering energy of 2.207 J/cm2, the ε and α' martensite phases appear due to relatively low SFE value in the austenitic stainless steel Cr-Mn specimen (10.9 mJ/m2) with the strain rate of 6.2 s-1 [16].

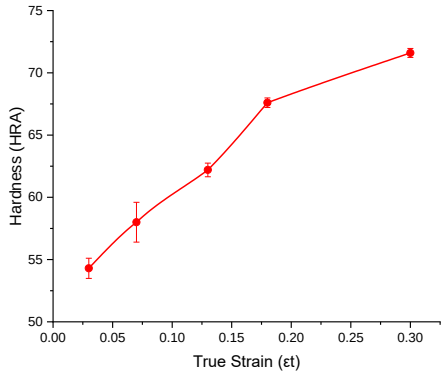

Figure 5. Hardness vs. true strain curve of low alloy austenitic stainless steel Cr-Mn after repetitive hammering

Also, with hammering energy of 2.207 J/cm^2, the ε and α' martensite phases appear due to relatively low SFE value in the austenitic stainless steel Cr-Mn specimen (10.9 mJ/m^2) with the strain rate of 6.2 s^{-1} [16].

Table 4 shows the impact energy of 11,330 J/cm^2, an increased FWHM (full width at half maximum) value from 0.452 to 0.483 compared to the initial material at hkl (111), indicates a widening and shift of the diffraction peaks caused by the formation of nano-twins measuring about 5 nm and the increasing density of stacking faults [33]-[34].

Nano-twin and stacking faults are planar defects that cause lattice parameters to change. Therefore, it causes a strain field to cause a shift and widening of the diffraction peak [9], [35]-[36].

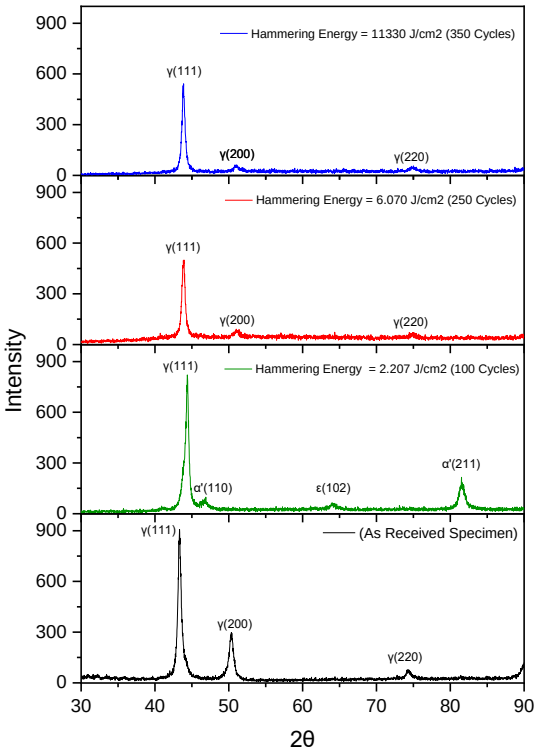

Figure 6. XRD result on as-received material, 100 hammering cycle (2207 J/cm^2 hammering energy), 250(6070 J/cm^2 hammering energy), and 350 hammering cycle (11330 J/cm^2 hammering energy) low alloy austenitic stainless-steel Cr-Mn

The formation of nano-twins can occur due to mechanical twinning in the repetitive hammering process.

Table 4. FWHM of as-received material, 100 hammering cycle (2207 J/cm^2 hammering energy), 250(6070 J/cm^2 hammering energy), and 350 hammering cycle (11330 J/cm^2 hammering energy) low alloy austenitic stainless steel Cr-Mn

Austenitic SS Cr-Mn Treatment	2θ	Hkl	FWHM
Solution annealing	43.4	(111)	0.452
	50.3	(200)	0.675
	74.4	(220)	1.024
Hammering energy 2207 J/cm^2	44.4	(111)	0.479
	46.9	(110)	-0.050
	64.0	(102)	1.066
	81.5	(211)	0.708
Hammering energy 6070 J/cm^2	43.9	(111)	0.411
	51.0	(200)	1.211
	74.9	(220)	0.921
Hammering energy 11330 J/cm^2	43.9	(111)	0.483
	51.0	(200)	1.538
	75.0	(220)	1.192

At the same time, the stacking faults can appear because the SFE value of the austenitic Cr-Mn stainless steel of 10.9 mJ/m^2 is relatively low. Thus, it is easier to form more stacking faults on the Cr-Mn austenitic stainless steel along with the given deformation widening of the diffraction peaks on the material from the repetitive hammering with the energy 11330 J/cm^2. The XRD analysis supports the microstructure analysis results. It shows that the increase in hardness in Cr-Mn austenitic stainless steels resulting from repetitive hammering is caused by strain hardening and an indication of mechanical twinning that forms nano-twin grains stacking faults. The sign of the presence of nano-twin shows the success of the dynamic plastic deformation process using repetitive hammering [33]-[34].

4. CONCLUSIONS

Repetitive hammering process up to 350 hammering cycles (11030 J/cm^2 hammering energy) can cause the formation of slip band, cross band, and wavy band with the indication of the nano-twin presence on the Cr-Mn austenitic stainless steel. The repetitive hammering process also increased the hardness from 53.5 HRA to 71.6 HRA, which shows the success of strengthening Cr-Mn austenitic stainless steel through the dynamic plastic deformation induced by repetitive hammering.

ACKNOWLEDGMENT

This research was financially supported by the Faculty of Mechanical and Aerospace Engineering, Institut Teknologi Bandung.

REFERENCES

[1] M. F. McGuire, *Stainless steels for design engineers*. Asm International, pp. 1 - 10; 69-90, 2008.

[2] A. Amininejad, R. Jamaati, and S. J. Hosseinipour, "Achieving superior strength and high ductility in AISI 304 austenitic stainless steel via asymmetric cold rolling," *Mater. Sci. Eng. A*, vol. 767, pp. 138433, 2019.

[3] A. Di Schino, "Manufacturing and application of stainless steels," *Manuf. Appl. Stainl. Steels*, pp. 7-9, 2020. Doi: 10.3390/books978-3-03928-651-5.

[4] D. Molnár, X. Sun, S. Lu, W. Li, G. Engberg, and L. Vitos, "Effect of temperature on the stacking fault energy and deformation behaviour in 316L austenitic stainless steel," *Mater. Sci. Eng. A*, vol. 759, no. May, pp. 490-497, 2019. Doi: 10.1016/j.msea.2019.05.079.

[5] D. Xu, X. Wan, J. Yu, G. Xu, and G. Li, "Effect of cold deformation on microstructures and mechanical properties of austenitic stainless steel," *Metals (Basel).*, vol. 8, no. 7, p. 522, 2018. Doi: 10.3390/met8070522.

[6] G. G. Maier and E. G. Astafurova, "A comparison of strengthening mechanisms of austenitic Fe-13Mn-1.3 C steel in warm and cold high-pressure torsion," *Metals (Basel).*, vol. 10, no. 4, p. 493, 2020.

[7] F. K. Yan, G. Z. Liu, N. R. Tao, and K. Lu, "Strength and ductility of 316L austenitic stainless steel strengthened by nano-scale twin bundles," *Acta Mater.*, vol. 60, no. 3, pp. 1059-1071, 2012.

[8] G. M. de Bellefon, J. C. Van Duysen, and K. Sridharan, "Composition-dependence of stacking fault energy in austenitic stainless steels through linear regression with random intercepts," *J. Nucl. Mater.*, vol. 492, pp. 227-230, 2017.

[9] P. Uttam, V. Kumar, K. H. Kim, and A. Deep, "Nanotwinning: Generation, properties, and application," *Mater. Des.*, vol. 192, pp. 108752, 2020. Doi: 10.1016/j.matdes.2020.108752.

[10] K. Lu, F. K. Yan, H. T. Wang, and N. R. Tao, "Strengthening austenitic steels by using nanotwinned austenitic grains," *Scr. Mater.*, vol. 66, no. 11, pp. 878-883, 2012.

[11] S. Wang, K. Wei, J. Li, Y. Liu, Z. Huang, Q. Mao, and Y. Li, "Enhanced tensile properties of 316L stainless steel processed by a novel ultrasonic resonance plastic deformation technique," *Mater. Lett.*, vol. 236, pp. 342-345, 2019. Doi: 10.1016/j.matlet.2018.10.080.

[12] A. K. Agrawal and A. Singh, "Limitations on the hardness increase in 316L stainless steel under dynamic plastic deformation," *Mater. Sci. Eng. A*, vol. 687, pp. 306-312, 2017.

[13] H. T. Wang and N. R. Tao, "Nano-twinned Fe-Mn alloy prepared by reverse martensitic phase transformation," *Scr. Mater.*, vol. 145, pp. 109-112, 2018. Doi: 10.1016/j.scriptamat.2017.10.024.

[14] J. Li, Y. Cao, B. Gao, Y. Li, and Y. Zhu, "Superior strength and ductility of 316L stainless steel with heterogeneous lamella structure," *J. Mater. Sci.*, vol. 53, no. 14, pp. 10442-10456, 2018. Doi: 10.1007/s10853-018-2322-4.

[15] C. Haase, D. A. Molodov, and W. Bleck,

"Texture and microstructure evolution during deformation and annealing of high-manganese TWIP steels," Lehrstuhl und Institut für Eisenhüttenkunde, 2016.

[16] S.-J. Lee, Y. Sun, and H. Fujii, "Stacking-fault energy, mechanical twinning and strain hardening of Fe-18Mn-0.6 C-(0, 1.5) Al twinning-induced plasticity steels during friction stir welding," *Acta Mater.*, vol. 148, pp. 235-248, 2018.

[17] W. Bleck, X. Guo, and Y. Ma, "The TRIP effect and its application in cold formable sheet steels," *Steel Res. Int.*, vol. 88, no. 10, pp. 1700218, 2017.

[18] R. Kartikasari, A. E. Wijaya, A. D. Iskandar, S. Subardi, and T. Triyono, "Mechanical properties and corrosion resistance of grinding ball Fe-xMn-10Al-1.25C alloys," *J. Phys. Conf. Ser.*, vol. 1375, no. 1, 2019. Doi: 10.1088/1742-6596/1375/1/012076.

[19] G. Meric de Bellefon, M. N. Gussev, A. D. Stoica, J. C. van Duysen, and K. Sridharan, "Examining the influence of stacking fault width on deformation twinning in an austenitic stainless steel," *Scr. Mater.*, vol. 157, pp. 162-166, 2018. Doi: 10.1016/j.scriptamat.2018.08.012.

[20] J. Zhang, Y. He, Y. Wang, Y. Wang, and T. Wang, "Influence of annealing temperature on microstructure, tensile properties and tensile deformation mechanism of metastable austenitic stainless steel repetitively cold-rolled and annealed," *Materialia*, vol. 8, 2019. Doi: 10.1016/j.mtla.2019.100455.

[21] R. E. Smallman and R. J. Bishop, *Modern physical metallurgy and materials engineering*. Butterworth-Heinemann, pp. 221-224; 297-299, 1999.

[22] H. S. Noh, J. H. Kang, K. M. Kim, and S. J. Kim, "Different effects of Ni and Mn on thermodynamic and mechanical stabilities in Cr-Ni-Mn austenitic steels," *Metall. Mater. Trans. A Phys. Metall. Mater. Sci.*, vol. 50, no. 2, pp. 616-624, 2019. Doi: 10.1007/s11661-018-5042-0.

[23] H. S. Noh, J. H. Kang, K. M. Kim, and S. J. Kim, "The effects of replacing Ni with Mn on hydrogen embrittlement in Cr-Ni-Mn-N austenitic steels," *Corros. Sci.*, vol. 152, pp. 93-100, 2019. Doi: 10.1016/j.corsci.2019.03.012.

[24] M. Khorrami, A. Z. Hanzaki, H. R. Abedi, M. Moallemi, J. Mola, and G. Chen, "On the effect of Mn-content on the strength-ductility balance in Ni-free high N transformation induced plasticity steels," *Mater. Sci. Eng. A*, vol. 814, pp 141260, 2021. Doi: 10.1016/j.msea.2021.141260.

[25] H. L. Yan, Y. Zhao, H. X. Liu, M. J. Zhang, H. F. Zhang, J. Bai, N. Jia, B. Yang, Z. B. Li, Y. D. Zhang, C. Esling, X. Zhao, and L. Zuo, "Ab-initio revelation on the origins of Ti substitution for Ga, Mn and Ni on ferromagnetism, phase stability and elastic properties in Ni2MnGa," *J. Alloys Compd.*, vol. 821, pp. 153481, 2020. Doi: 10.1016/j.jallcom.2019.153481.

[26] A. Weidner, J. Man, W. Skrotzki, and J. Polák, "Slip localization and dislocation structure at early stages of fatigue damage in austenitic stainless steel (316L)," *ICF12, Ottawa*, vol. 2013, 2009.

[27] B. Poole and F. P. E. Dunne, "Slip band interactions and GND latent hardening in a galling resistant stainless steel," *Mater. Sci. Eng. A*, vol. 813, pp. 141176, 2021. Doi: 10.1016/j.msea.2021.141176.

[28] R. Ke, X. Wan, Y. Zhang, C. Hu, and K. Wu, "Insight in the impact of pre-deformation on structure - deformation - property relationship in Cr-Mn-N stainless steel," *Mater. Charact.*, pp. 111689, 2021. Doi: 10.1016/j.matchar.2021.111689.

[29] H. Kamali, H. Xie, H. Bi, E. Chang, H. Xu, H. Yu, and Z. Jiang, "Deformation mechanism and texture evolution of a low-Ni Cr–Mn–N austenitic stainless steel under bending deformation," *Mater. Sci. Eng. A*, vol. 804, pp. 140724, 2021. Doi: 10.1016/j.msea.2020.140724.

[30] A. A. Tiamiyu, V. Tari, J. A. Szpunar, A. G. Odeshi, and A. K. Khan, "Effects of grain refinement on the quasi-static compressive behavior of AISI 321 austenitic stainless steel: EBSD, TEM, and XRD studies," *Int. J. Plast.*, vol. 107, pp. 79-99, 2018. Doi: 10.1016/j.ijplas.2018.03.014.

[31] A. Grajcar, A. Kozłowska, and B. Grzegorczyk, "Strain hardening behavior and microstructure evolution of high-manganese steel subjected to interrupted tensile tests," *Metals (Basel).*, vol. 8, no. 2, 2018. Doi: 10.3390/met8020122.

[32] Y. Hong, C. Zhou, Y. Zheng, L. Zhang, J. Zheng, X. Chen, and B. An, "Formation of strain-induced martensite in selective laser melting austenitic stainless steel," *Mater. Sci. Eng. A*, vol. 740-741, pp. 420-426, 2019. Doi: 10.1016/j.msea.2018.10.121.

[33] P. Muhammed Shafi and A. Chandra Bose, "Impact of crystalline defects and size on X-ray line broadening: A phenomenological approach for tetragonal SnO2 nanocrystals," *AIP Adv.*, vol. 5, no. 5, pp. 57137, 2015.

[34] B. Roy and J. Das, "Strengthening face centered cubic crystals by annealing induced nano-twins," *Sci. Rep.*, vol. 7, no. 1, pp. 1-8, 2017.

[35] L. Löffler and W. Mader, "Anisotropic X-ray diffraction peak broadening and twinning in diaspore-derived corundum," *J. Eur. Ceram. Soc.*, vol. 25, no. 5, pp. 639-648, 2005.

[36] Z. Pei, "An overview of modeling the stacking faults in lightweight and high-entropy alloys: Theory and application," *Mater. Sci. Eng. A*, vol. 737, no. September, pp. 132-150, 2018. Doi: 10.1016/j.msea.2018.09.028.

[37] W. Woo, J. S. Jeong, D. Kim, C. M. Lee, S. Choi, J. Suh, S. Y. Lee, S. Harjo, and T. Kawasaki, "Stacking fault energy analyses of additively manufactured stainless steel 316L and CrCoNi Medium entropy alloy using in situ neutron diffraction," *Sci. Rep.*, vol. 10, no. 1, pp. 2-4, 2020. Doi: 10.1038/s41598-020-58273-3.